Spectroelectrochemical (UV−Vis, IR, NMR, and EPR) Study of the Inorganometallic Complexes $Ru(E)(E')(CO)_2$(iPr-DAB) (E = Cl, E′ = $SnPh_3$, $PbPh_3$; E = Me, $SnPh_3$, $GePh_3$, E′ = $SnPh_3$; E = E′ = $PbPh_3$; iPr-DAB = 1,4-Diisopropyl-1,4-diaza-1,3-butadiene)

Maxim P. Aarnts,[†] František Hartl,*[,†] Karin Peelen,[†] Derk J. Stufkens,[†] Christian Amatore,[‡] and Jean-Noël Verpeaux[‡]

Anorganisch Chemisch Laboratorium, J. H. van't Hoff Research Instituut, Universiteit van Amsterdam, Nieuwe Achtergracht 166, 1018 WV Amsterdam, The Netherlands, and Ecole Normale Supérieure, Département de Chimie, URA CNRS 1679, 24 rue Lhomond, 75231 Paris Cedex 05, France

Received April 2, 1997[⊗]

The reduction paths of two series of inorganometallic Ru complexes, $Ru(Cl)(E')(CO)_2$(iPr-DAB) (E′ = $SnPh_3$, $PbPh_3$) and $Ru(E)(E')(CO)_2$(iPr-DAB) (E = Me, $GePh_3$, $SnPh_3$, E′ = $SnPh_3$; E = E′ = $PbPh_3$), were studied by a series of spectroelectrochemical techniques. Reduction of the Cl complexes is a two-electron ECE process which directly affords the closed-shell five-coordinate anions $[Ru(E')(CO)_2(iPr\text{-}DAB)]^-$ *via* transient radicals $[Ru(E')(CO)_2(iPr\text{-}DAB)]^{\bullet}$. In the final step of the overall ECEC sequence at room temperature the five-coordinate anions attack the parent complexes, producing the dimers $[Ru(E')(CO)_2(iPr\text{-}DAB)]_2$. In contrast, the non-halide complexes are reversibly reduced to the radical anions $[Ru(E)(E')(CO)_2(iPr\text{-}DAB)]^{\bullet-}$ whose stability arises from the strength of the delocalized axial E−Ru−E′ bond. Subsequent reduction of $[Ru(E')(CO)_2(iPr\text{-}DAB)]_2$ and $[Ru(E)(E')(CO)_2(iPr\text{-}DAB)]^{\bullet-}$ ultimately yields $[Ru(E')(CO)_2(iPr\text{-}DAB)]^-$. Reverse oxidation of the anions directly results in the recovery of the parent complexes $Ru(Cl)(E')(CO)_2$(iPr-DAB) and $Ru(E)(E')(CO)_2$(iPr-DAB). Two different, temperature-controlled mechanisms operate during the oxidation of the Cl complexes. The electronic and geometric structures of $[Ru(E)(E')(CO)_2(iPr\text{-}DAB)]^{\bullet-}$ (E, E′ ≠ Cl) and $[Ru(E')(CO)_2(iPr\text{-}DAB)]^-$ are discussed on the basis of their UV−vis, IR, NMR, EPR, and resonance Raman data.

Introduction

The photochemical, photophysical, and redox properties of the complexes $[M(E)(CO)_3(\alpha\text{-diimine})]^n$ (M = Mn, Re; n = 0, +1; E = halide, alkyl, PR_3, donor solvent, etc.) were shown in numerous studies[1] to be strongly determined by the nature and combination of the α-diimine and the axial ligand E. In this respect the related complexes $[Ru(E)(E')(CO)_2(\alpha\text{-diimine})]^n$ are more versatile candidates for the widely ranged investigation of the energy- and electron-transfer reactions, luminescence properties, and radical reactivity, since both axial ligands E and E′ can be varied independently.[2]

Quite remarkably, a close correspondence has often been observed between the photochemical behavior of this class of metal(diimine) complexes and their reactivity in the reduced state, although the operating mechanisms may differ. Examples are (i) the photochemical and electrochemical reduction of CO_2 catalyzed by $Re(E)(CO)_3(bpy)$,[1e,3] $[Ru(CO)_2(bpy)_2]^{2+}$, and $Ru(Cl)_2(CO)_2(bpy)$ (bpy = 2,2′-bipyridine),[4] (ii) the liberation of alkyl radicals R• on MLCT (metal-to-ligand charge transfer) excitation and/or electrochemical reduction of Mn(R)-

[†] Universiteit van Amsterdam.
[‡] Ecole Normale Supérieure.
[⊗] Abstract published in *Advance ACS Abstracts,* September 15, 1997.

(1) (a) Aarnts, M. P.; Wilms, M.; Stufkens, D. J.; Baerends, E. J.; Clark, I.; George, M. W.; Turner, J. J.; Vlček, A., Jr. *Chem. Eur. J.* **1996**, *2*, 1556 and ref 7−28 therein. (b) Kleverlaan, C. J.; Martino, D. M.; van Willigen, H.; Stufkens, D. J.; Oskam, A. *J. Phys. Chem.* **1996**, *100*, 18607. (c) Wallace, L.; Woods, C.; Rillema, D. P. *Inorg. Chem.* **1995**, *34*, 2875. (d) Rossenaar, B. D.; Kleverlaan, C. J.; van de Ven, M. C. E.; Stufkens, D. J.; Vlček, A., Jr. *Chem. Eur. J.* **1996**, *2*, 228. (e) Johnson, F. P. A.; George, M. W.; Hartl, F.; Turner, J. J. *Organometallics* **1996**, *15*, 3374 and ref 1−14 therein. (f) Rossenaar, B. D.; Hartl, F.; Stufkens, D. J. *Inorg. Chem.* **1996**, *35*, 6194. (g) Lee, Y. F.; Kirchhoff, J. R.; Berger, R. M.; Gosztola, D. *J. Chem. Soc., Dalton Trans.* **1995**, 3677. (h) Klein, A.; Vogler, C.; Kaim, W. *Organometallics* **1996**, *15*, 236. (i) Rossenaar, B. D.; Stufkens, D. J.; Oskam, A.; Fraanje, J.; Goubitz, K. *Inorg. Chim. Acta* **1996**, *247*, 215. (j) Brown, N. C.; Carriedo, G. A.; Connelly, N. G.; García Alonso, F. J.; Quarmby, I. C.; Rieger, A. L.; Rieger, P. H.; Riera, V.; Vivanco, M. *J. Chem. Soc., Dalton Trans.* **1994**, 3745.

(2) (a) Nieuwenhuis, H. A.; Stufkens, D. J.; Vlček, A., Jr. *Inorg. Chem.* **1995**, *34*, 3879. (b) Nieuwenhuis, H. A.; Stufkens, D. J.; McNicholl, R.; Al-Obaidi, A. H.; Coates, C. G.; Bell, S. E. J.; McGarvey, J. J.; Westwell, J.; George, M. W.; Turner, J. J. *J. Am. Chem. Soc.* **1995**, *117*, 5579. (c) Nieuwenhuis, H. A.; Stufkens, D. J.; Oskam, A. *Inorg. Chem.* **1994**, *33*, 3212. (d) Nieuwenhuis, H. A.; van Loon, A.; Moraal, M. A.; Stufkens, D. J.; Oskam, A.; Goubitz, K. *J. Organomet. Chem.* **1995**, *492*, 165. (e) Nieuwenhuis, H. A.; van de Ven, M. C. E.; Stufkens, D. J.; Oskam, A.; Goubitz, K. *Organometallics* **1995**, *14*, 780. (f) Nieuwenhuis, H. A.; van Loon, A.; Moraal, M. A.; Stufkens, D. J.; Oskam, A.; Goubitz, K. *Inorg. Chim. Acta* **1995**, *232*, 19.

(3) (a) Kutal, C.; Corbin, J.; Ferraudi, G. *Organometallics* **1987**, *6*, 553. (b) Calzaferri, G.; Hadener, K.; Li, J. *J. Photochem. Photobiol., A: Chem.* **1992**, *64*, 259. (c) Hawecker, J.; Lehn, J.-M., Ziessel, R. *Helv. Chim. Acta* **1986**, *69*, 1990.

(4) (a) Ishida, H.; Tanaka, K.; Tanaka, T. *Organometallics* **1987**, *6*, 181. (b) Ishida, H.; Fujiki, K.; Ohba, T.; Ohkubo, K.; Tanaka, K.; Terada, T.; Tanaka, T. *J. Chem. Soc., Dalton Trans.* **1990**, 2155. (c) Nagao, H.; Mizukawa, T.; Tanaka, K. *Inorg. Chem.* **1994**, *33*, 3415. (d) Chardon-Noblat, S.; Collomb-Dunand-Sauthier, M.-N.; Deronzier, A.; Ziessel, A.; Zsoldos, D. *Inorg. Chem.* **1994**, *33*, 4410. (e) Collomb-Dunand-Sauthier, M.-N.; Deronzier, A. *J. Organomet. Chem.* **1993**, *444*, 191. (f) Collomb-Dunand-Sauthier, M.-N.; Deronzier, A.; Ziessel, A. *Inorg. Chem.* **1994**, *33*, 2961. (g) Lehn, J.-M.; Ziessel, R. *J. Organomet. Chem.* **1990**, *382*, 157.

S0276-7333(97)00280-X CCC: $14.00

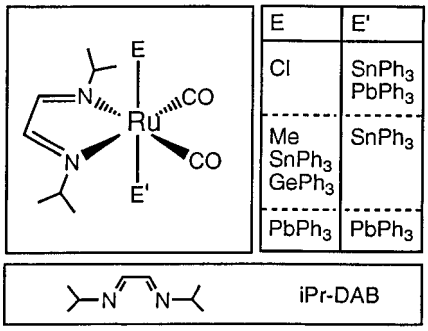

Figure 1. Schematic structure of the Ru(E)(E′)(CO)$_2$(iPr-DAB) complexes.

(CO)$_3$(iPr-DAB),[1i,5] and (iii) the photo and electrochemical generation of the five-coordinate anion [Mn(CO)$_3$(bpy)]$^-$ from Mn(Br)(CO)$_3$(bpy).[1f,5,6]

An interesting situation arises when the M(E)(CO)$_3$(α-diimine) (M = Mn, Re) or Ru(E)(E′)(CO)$_2$(α-diimine) complexes contain axial ligand(s) E and E′, usually alkyls or (carbonyl)metal fragments, covalently bound by relatively high-lying $\sigma_{(MC)}$ or $\sigma_{(MM')}$ orbitals. The coordination of such ligands profoundly affects the bonding properties of the metal(α-diimine) fragment and, hence, the spectroscopic and redox properties of the complexes.[1i,7] We have recently demonstrated this approach in a spectroelectrochemical and theoretical DFT-MO study of the inorganometallic complex Ru(SnPh$_3$)$_2$(CO)$_2$(iPr-DAB) and its stable radical anion.[8] In these compounds, strong mixing between the $\pi^*_{(iPr-DAB)}$ and occupied weakly bonding $\sigma_{(Sn-Ru-Sn)}$ (*i.e.*, Ru(p_z) + Sn(sp^3-sp^3)) orbitals results in unusual extensive $\sigma-\pi^*$ electron delocalization. This stabilizing delocalization becomes diminished when one of the axial SnPh$_3$ ligands is replaced, for example, by a halide, causing quite different *excited-state* properties of these complexes.[1a]

The principle subject of this study was to establish differences in the *redox properties and reactivity* between the halide complexes Ru(Cl)(E′)(CO)$_2$(iPr-DAB), E′ = SnPh$_3$, PbPh$_3$, Me,[9,10] with largely localized σ,π-(Cl−Ru−E′) and π^*(iPr-DAB) systems and the strongly $\sigma\pi^*$-delocalized non-halide derivatives Ru(E)(E′)(CO)$_2$(iPr-DAB) (E = Me, SnPh$_3$, PbPh$_3$, E′ = SnPh$_3$; E = E′ = PbPh$_3$), see Figure 1. We have also attempted to characterize most of the detectable reduction products, in particular their spectroscopic (IR, UV−vis, NMR, EPR) properties, molecular geometry, and the E,E′-dependent electron density distribution.

Experimental Section

Materials. The solvents acetonitrile (MeCN, Fluka) and THF (Acros Chimica) were dried on CaH$_2$ and Na wire, respectively, and distilled under nitrogen *prior* to use. The supporting electrolyte Bu$_4$NPF$_6$ (Fluka) was dried overnight under vacuum at 180 °C and stored under argon. Ferrocene (Fc, BDH) was used as received.

Syntheses, X-ray structures, and spectroscopic data of the complexes under study have been reported elsewhere.[7b,8]

Spectroelectrochemical samples were prepared under an atmosphere of dry nitrogen or argon, using Schlenk techniques. Solutions of the light-sensitive complexes Ru(E)(E′)(CO)$_2$(iPr-DAB), E,E′ ≠ Cl, were handled in the dark or in light-protected cells.

Spectroscopic and Spectroelectrochemical Measurements and Instrumentation. IR spectra were recorded on a Bio-Rad FTS-7 spectrometer with a resolution of 2 cm^{-1}. Electronic absorption spectra were measured on a Perkin-Elmer Lambda 5 UV−vis spectrophotometer linked to a 3600 data station. Resonance Raman measurements were performed on a DILOR X4 spectrometer, using a SP model 2016 Ar$^+$ laser as the excitation source. ^{1}H and ^{13}C NMR measurements were carried out on a Bruker AMX 300 spectrometer and ^{119}Sn NMR measurements on a Bruker WM 250 spectrometer. The NMR samples of [Ru(SnPh$_3$)(CO)$_2$(iPr-DAB)]$_2$ and [Ru(SnPh$_3$)(CO)$_2$(iPr-DAB)]$^-$ were prepared in a gastight reaction vessel with an attached NMR tube. In this vessel, *ca.* 10^{-1} M Ru(Cl)(SnPh$_3$)(CO)$_2$(iPr-DAB) in THF-d$_8$ was reduced by 1% Na(Hg) until the color changed from orange-yellow to the green color of the dimer, and further to the deep red color of the anion. The NMR tube with the sample was finally sealed off. X-band EPR spectra were recorded at room temperature on a Bruker ECS 106 spectrometer with a field modulation of 100 KHz. The frequency was measured with a HP5350B microwave frequency counter. The magnetic field was calibrated with an AEG magnetic field meter. The microwave power incident to the cavity was measured with a HP432B power meter. The EPR measurements were carried out in a gastight EPR tube attached to a reaction vessel in which 10^{-3} M solutions of the parent complexes in THF were chemically reduced by 1% Na(Hg) until the color changed from red to the green color of the radical anions [Ru(E)(E′)(CO)$_2$(iPr-DAB)]$^{\bullet-}$ (E = E′ = SnPh$_3$, PbPh$_3$) and from red to the orange color of [Ru(E)(SnPh$_3$)(CO)$_2$(iPr-DAB)]$^{\bullet-}$ (E = GePh$_3$, Me). The end of the reduction was independently checked by IR and UV−vis spectroscopy. The EPR-simulations[11] program was used to simulate the experimental spectra.

IR and UV−vis spectroelectrochemical measurements were performed with an optically transparent thin-layer electrochemical (OTTLE) cell,[12] following a procedure described elsewhere.[5]

Cyclic Voltammetry and Chronoamperometry. Cyclic voltammograms were recorded in a light-protected cell equipped with a Pt disk working electrode (d = 500 μm) polished with a 0.25 μm diamond paste between scans, a Pt gauze auxiliary electrode, and SCE (Tacussel) normal reference or coiled Ag wire pseudoreference electrodes. The standard ferrocene/ferrocenium (Fc/Fc$^+$) redox couple[13] served as an internal potential reference. A home-built potentiostat equipped with a positive feedback for ohmic-drop compensation was used.[14] The potential−time wave forms were provided by an EG & G PAR model 175 signal generator. A Nicolet 3091 digital oscilloscope was used to store the voltammograms and chronoamperograms and to read their current/potential characteristics.

The apparent number of electrons (n_{app}) exchanged during the reduction of Ru(Cl)(SnPh$_3$)(CO)$_2$(iPr-DAB) at room tem-

(5) Rossenaar, B. D.; Hartl, F.; Stufkens, D. J.; Amatore, C.; Maisonhaute, E.; Verpeaux, J.-N. *Organometallics* **1997**, *16*, 4675.
(6) Stor, G. J.; Morrison, S. L.; Stufkens, D. J.; Oskam, A. *Organometallics* **1994**, *13*, 2641.
(7) (a) Aarnts, M. P.; Stufkens, D. J.; Oskam, A.; Fraanje, J.; Goubitz, K.; Veldman, N.; Spek, A. L. *J. Organomet. Chem.* **1997**, *531*, 191 and ref 23−35 therein. (b) Aarnts, M. P.; Stufkens, D. J.; Oskam, A.; Fraanje, J.; Goubitz, K. *Inorg. Chim. Acta* **1997**, *256*, 93.
(8) Aarnts, M. P.; Hartl, F.; Peelen, K.; Stufkens, D. J.; Fraanje, J.; Goubitz, K.; Wilms, M.; Baerends, E. J.; Vlček., A., Jr. *Inorg. Chem.*. **1996**, *35*, 5468.
(9) Hartl, F.; Luyten, H.; Nieuwenhuis, H. A.; Schoemaker, G. C. *Appl. Spectrosc.* **1994**, *48*, 1522.
(10) Nieuwenhuis, H. A. Ph.D. Thesis, University of Amsterdam, Amsterdam, The Netherlands, 1994.
(11) Bruns, W.; Schulz, A. *ESR-Simulation Program*; Universität Stuttgart: Stuttgart, Germany, 1991.
(12) Krejčík, M.; Daněk, M.; Hartl, F. *J. Electroanal. Chem., Interfacial Electrochem.* **1991**, *317*, 179.
(13) Gagné, R. R.; Koval, C. A.; Lisensky, G. C. *Inorg. Chem.* **1980**, *19*, 2854.
(14) Amatore, C.; Lefrou, C.; Pflüger, F. *J. Electroanal. Chem.* **1989**, *270*, 43.

Table 1. IR ν(CO) and Near-UV−Vis Data for the Title Complexes Ru(E)(E′)(CO)$_2$(iPr-DAB) and Their Reduction Products[a]

complex	IR ν(CO) (cm^{-1})	IR k^b (Nm^{-1})	UV−vis λ_{max} (ϵ^c), (nm) (cm^{-1} M^{-1})
Ru(Cl)(PbPh$_3$)(CO)$_2$(iPr-DAB)	2026, 1970	1612	439 (2520)
Ru(Cl)(SnPh$_3$)(CO)$_2$(iPr-DAB)	2025, 1964	1607	429 (2850)
Ru(I)(Me)(CO)$_2$(iPr-DAB)[d]	2024, 1958	1602	374 (2630), 447 (1550)
Ru(PbPh$_3$)$_2$(CO)$_2$(iPr-DAB)	2004, 1953	1581	540 (4840)
Ru(GePh$_3$)(SnPh$_3$)(CO)$_2$(iPr-DAB)	2005, 1949	1579	514 (5130)
Ru(SnPh$_3$)$_2$(CO)$_2$(iPr-DAB)	2003, 1950	1578	511 (6050)
Ru(Me)(SnPh$_3$)(CO)$_2$(iPr-DAB)	2003, 1945	1574	513 (5720)
[Ru(PbPh$_3$)(CO)$_2$(iPr-DAB)]$_2$	1987, 1965, 1935		416, 685
[Ru(SnPh$_3$)(CO)$_2$(iPr-DAB)]$_2$	1988, 1963, 1934		385 (16500), 513 (3280), 687 (19800)
[Ru(Me)(CO)$_2$(iPr-DAB)]$_2$[d]	1982, 1954, 1924		405 (4520), 563 (2480), 745 (29000)
[Ru(PbPh$_3$)$_2$(CO)$_2$(iPr-DAB)]$^{\bullet-}$	1980, 1916	1533	441 (2600), 812 (2750)
[Ru(SnPh$_3$)$_2$(CO)$_2$(iPr-DAB)]$^{\bullet-}$	1975, 1910	1524	454 (3300), 652 (1900)
[Ru(GePh$_3$)(SnPh$_3$)(CO)$_2$(iPr-DAB)]$^{\bullet-}$	1976, 1909	1524	457 (2570), 641 (1220)
[Ru(Me)(SnPh$_3$)(CO)$_2$(iPr-DAB)]$^{\bullet-}$	1965, 1891	1502	382 (3200), 428 (3300)
[Ru(PbPh$_3$)(CO)$_2$(iPr-DAB)]$^-$	1926, 1859	1447	540
[Ru(SnPh$_3$)(CO)$_2$(iPr-DAB)]$^-$	1924, 1856	1443	503 (10100)
Na$^+$[Ru(SnPh$_3$)(CO)$_2$(iPr-DAB)]$^-$ [e,f]	1923, 1858, 1833		503
[Ru(Me)(CO)$_2$(iPr-DAB)]$^-$ [d]	1915, 1835	1420	500 (8100)
[Mn(CO)$_3$(iPr-DAB)]$^-$ [g]	1919, 1811	1379	392 (6550), 490 (9300)

[a] In THF at room temperature, unless stated otherwise. [b] CO force constant, calculated according to $5.889 \times 10^{-5}(\nu_1^2 + \nu_2^2) = 0.14583(k + k_i)$ and $5.889 \times 10^{-5}(\nu_1^2 - \nu_2^2) = 0.14583(k - k_i)$ (k_i = interaction constant, ν_1 and ν_2 are the frequencies of the ν_s(CO) and ν_{as}(CO) modes, respectively).[32] [c] Molar absorption coefficients in brackets. [d] Taken from refs 9 and 10. [e] Reduction of Ru(Cl)(SnPh$_3$)(CO)$_2$(iPr-DAB) by 1% Na(Hg). [f] Resonance Raman spectrum measured in THF at room temperature, using $\lambda_{exc} = 488$ nm. Resonantly enhanced bands observed at 1471, 1275, 949, 904, 828, and 601 cm^{-1}. [g] Taken from ref 5.

perature was determined employing a literature method which combines chronoamperometry and steady-state voltammetry at ultramicroelectrodes.[15] The experiment was performed with 1.73×10^{-3} M Ru(Cl)(SnPh$_3$)(CO)$_2$(iPr-DAB) and 1.18×10^{-3} M Fc in MeCN/0.3 M Bu$_4$NPF$_6$, following an identical two-step procedure as described in detail for [Mn(E)(CO)$_3$(iPr-DAB)]^n (n = 0, E = Br; n = +1, E = THF, MeCN) in the companion article.[5]

(i) Chronoamperometry at a Pt disk electrode ($d = 500\ \mu$m) afforded the averaged value R_{chrono}[5,15] $= n_{app}(D_{Ru}/D_{Fc})^{1/2} = 0.77 \pm 0.02$, where D_{Ru} and D_{Fc} are the diffusion coefficients of Ru(Cl)(SnPh$_3$)(CO)$_2$(iPr-DAB) and ferrocene, respectively.

(ii) The same chronoamperometric experiment performed with a Pt disk ultramicroelectrode ($d = 20\ \mu$m) under a spheric diffusion regime[5] resulted in R_{lim}[15] $= n_{app}(D_{Ru}/D_{Fc}) = 0.455$. Steady-state voltammetry[15] could not be employed in this case due to strong adsorption of the RuCl complex at the Pt ultramicroelectrode, which caused dubious voltammetric current responses. Using the reported D_{Fc} value in MeCN (1.9×10^{-5} cm^2 s^{-1})[15,16] and combining the expressions for R_{lim} and R_{chrono} gives $n_{app} = 1.3 \pm 0.1$ and $D_{Ru} = (0.34 \pm 0.02)D_{Fc} = 6.46 \times 10^{-6}$ cm^2 s^{-1}.[17] These data are validated by the good match of the characteristic time for the steady-state measurement at the Pt ultramicroelectrode $T_c = (d/2)^2/D_{Ru} = 155$ ms, with $T_c = 50-500$ ms (pulse duration) chosen for the transient chronoamperometric experiments. In the cyclic voltammetry, the determined value $n_{app} = 1.3$ corresponds to the reduction of Ru(Cl)(SnPh$_3$)(CO)$_2$(iPr-DAB) studied at $v = 100-200$ mV/s (see Results).

Computational Details. All DFT-MO calculations were performed using the Amsterdam density functional program package ADF.[18] Details of the DFT-MO calculations on the complexes studied in this article have been described elsewhere.[1a,8] The EPR parameters of the radical anions [Ru(E)(E′)(CO)$_2$(iPr-DAB)]$^{\bullet-}$, E ≠ Cl, were calculated using the program GATENQ[19] and considering Fermi contact terms and dipolar interactions.

Results

UV−Vis and IR Spectroelectrochemistry of Ru(Cl)(E′)(CO)$_2$(iPr-DAB) (E′ = SnPh$_3$, PbPh$_3$). The UV−vis and IR spectral data of the starting compounds Ru(Cl)(E′)(CO)$_2$(iPr-DAB) (E′ = SnPh$_3$, PbPh$_3$) and their reduction products are summarized in Table 1. Reduction of Ru(Cl)(SnPh$_3$)(CO)$_2$(iPr-DAB) at 293 K resulted in the disappearance of the visible absorption band at 429 nm and simultaneous growth of three new bands at 385, 513, and 687 nm, see Figure 2 (left). Monitoring this cathodic step with IR spectroscopy revealed new ν(CO) bands at 1988, 1963, and 1934 cm^{-1}, see Figure 2 (right). These UV−vis and IR data strongly resemble those reported for the metal−metal-bonded dimer [Ru(Me)(CO)$_2$(iPr-DAB)]$_2$ with an eclipsed conformation of the iPr-DAB ligands, see Table 1.[9,10,20] We, therefore, conclude that the reduction of Ru(Cl)(SnPh$_3$)(CO)$_2$(iPr-DAB) produces the corresponding dimer [Ru(SnPh$_3$)(CO)$_2$(iPr-DAB)]$_2$. Notably, this compound is also produced during photolysis of Ru(E)(SnPh$_3$)(CO)$_2$(iPr-DAB) (E = Me, Mn(CO)$_5$, Re(CO)$_5$).[21]

Subsequent reduction of [Ru(SnPh$_3$)(CO)$_2$(iPr-DAB)]$_2$ afforded a single carbonyl product (ν(CO) at 1924 and 1856 cm^{-1}) strongly absorbing in the visible region at 500 nm, see Figure 2. It is assigned as being due to the five-coordinate anion [Ru(SnPh$_3$)(CO)$_2$(iPr-DAB)]$^-$. This assignment has been based on the close correspondence with the UV−vis and IR spectra of the derivative [Ru(Me)(CO)$_2$(iPr-DAB)]$^-$, see Table 1.[9,10,20] Reoxidation of [Ru(SnPh$_3$)(CO)$_2$(iPr-DAB)]$^-$ gave back the dimer [Ru(SnPh$_3$)(CO)$_2$(iPr-DAB)]$_2$, which further

(15) Amatore, C.; Azzabi, M.; Calas, P.; Jutand, A.; Lefrou, C.; Rollin, Y. *J. Electroanal. Chem., Interfacial Electrochem.* **1990**, *288*, 45.
(16) Scholl, H.; Sochaj, K. *Electrochim. Acta* **1991**, *36*, 689.
(17) The diffusion coefficient of Ru(Cl)(SnPh$_3$)(CO)$_2$(iPr-DAB) is smaller than that of related Mn(Br)(CO)$_3$(iPr-DAB) ($D_{MnBr} = 1.03 \times 10^{-5}$ cm^2 s^{-1}) determined in the same way,[5] in line with the apparently larger size of the former complex.
(18) (a) Baerends, E. J.; Ellis, D. E.; Ros, P. *Chem. Phys.* **1973**, *2*, 52. (b) Baerends, E. J.; Ros, P. *Int. J. Quantum Chem.* **1978**, *S12*, 169.
(19) Belanzoni, P.; Baerends, E. J.; van Asselt, S.; Langewen, P. B. *J. Phys. Chem.* **1995**, *99*, 13094.
(20) tom Dieck, H.; Rohde, W.; Behrens, U. *Z. Naturforsch.* **1989**, *44b*, 158.
(21) Aarnts, M. P.; Stufkens, D. J.; Vlček, A., Jr. *Inorg. Chim. Acta*, in press.

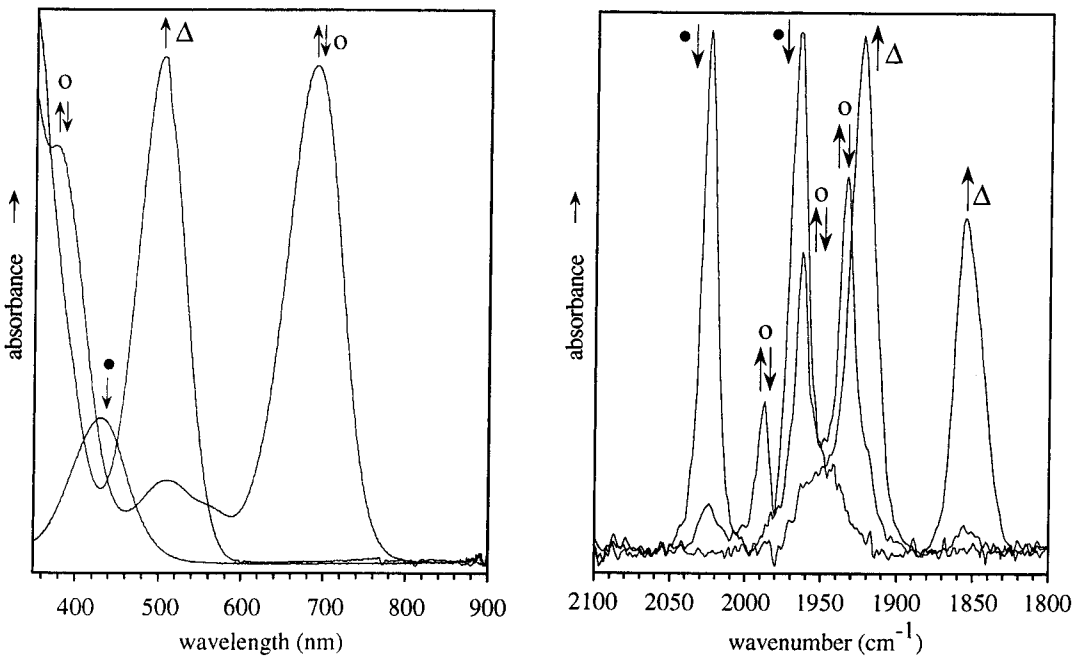

Figure 2. UV−vis spectra (left) and IR spectra in the carbonyl stretching region (right) of (●) the complex Ru(Cl)(SnPh$_3$)(CO)$_2$(iPr-DAB) and its one-electron- and two-electron-reduced products, *viz.* (○) the dimer [Ru(SnPh$_3$)(CO)$_2$(iPr-DAB)]$_2$, and (△) the five-coordinate anion [Ru(SnPh$_3$)(CO)$_2$(iPr-DAB)]$^-$, respectively. Conditions: THF, 293 K, electrolysis within an OTTLE cell.[12]

oxidizes to recover the parent complex Ru(Cl)(SnPh$_3$)(CO)$_2$(iPr-DAB) in high yield. An identical route was followed on reduction of Ru(Cl)(PbPh$_3$)(CO)$_2$(iPr-DAB), see Table 1.

The complex Ru(Cl)(SnPh$_3$)(CO)$_2$(iPr-DAB) and its two diamagnetic reduction products [Ru(SnPh$_3$)(CO)$_2$(iPr-DAB)]$_2$ and [Ru(SnPh$_3$)(CO)$_2$(iPr-DAB)]$^-$ were also characterized by ^{1}H, ^{13}C, and ^{119}Sn NMR spectroscopy, see Table 2 and Figure 3 (Supporting Information). A sufficiently high NMR concentration of the dimer and anion was achieved by reducing Ru(Cl)(SnPh$_3$)(CO)$_2$(iPr-DAB) stepwise with 1% Na(Hg). A detailed interpretation of the NMR data of [Ru(SnPh$_3$)(CO)$_2$(iPr-DAB)]$^-$ is given in the Discussion. For comparison, NMR spectra of Ru(SnPh$_3$)$_2$(CO)$_2$(iPr-DAB)[7b,8] are also presented in Figure 3 and Table 2.

Cyclic Voltammetry and Reduction Path of Ru(Cl)(E′)(CO)$_2$(iPr-DAB) (E′ = SnPh$_3$, PbPh$_3$). The cyclic voltammetric responses of Ru(Cl)(E′)(CO)$_2$(iPr-DAB) (E′ = SnPh$_3$, PbPh$_3$) will be described in detail only for E′ = SnPh$_3$. The redox potentials of the complexes and their reduction products are summarized in Table 3.

The cyclic voltammogram of Ru(Cl)(SnPh$_3$)(CO)$_2$(iPr-DAB) in MeCN at room temperature shows two cathodic peaks, see Figure 4, and a totally chemically irreversible anodic process at $E_{p,a} = +0.80$ V ($\nu = 100$ mV/s) localized on the Ru−Cl moiety[1a] (not shown in Figure 4). The first cathodic step at $E_{p,c} = -1.48$ V, see Figure 4a, ultimately yields the metal−metal-bonded dimer [Ru(SnPh$_3$)(CO)$_2$(iPr-DAB)]$_2$ (see above). The second cathodic peak at $E_{p,c} = -1.57$ V ($\nu = 100$ mV/s) corresponds to the reduction of the dimer, producing the five-coordinate anion [Ru(SnPh$_3$)(CO)$_2$(iPr-DAB)]$^-$. After both cathodic steps are passed there are two anodic peaks observable on the scan reversal. In conformity with the thin-layer cyclic voltammogram of Ru(Cl)(SnPh$_3$)(CO)$_2$(iPr-DAB), recorded in the course of the UV−vis and IR OTTLE experiments, the anodic peak at $E_{p,a} = -1.07$ V ($\nu = 100$ mV/s) belongs to the chemically irreversible oxidation of the anion [Ru(SnPh$_3$)(CO)$_2$(iPr-DAB)]$^-$ and the more positive peak at $E_{p,a} = -0.16$ V to the chemically irreversible oxidation of the dimer [Ru(SnPh$_3$)(CO)$_2$(iPr-DAB)]$_2$. The latter anodic step leads to the recovery of parent Ru(Cl)(SnPh$_3$)(CO)$_2$(iPr-DAB).

Increasing the scan rate from 100 mV/s to 10 V/s resulted in diminished cathodic peak due to the reduction of the dimer and to increased anodic current due to the oxidation of [Ru(SnPh$_3$)(CO)$_2$(iPr-DAB)]$^-$, see Figures 4a−c. Importantly, the cyclic voltammogram of Ru(Cl)(SnPh$_3$)(CO)$_2$(iPr-DAB) recorded in THF at 223 K only showed the reduction of the parent complex and the reverse oxidation of [Ru(SnPh$_3$)(CO)$_2$(iPr-DAB)]$^-$. The cathodic and anodic peaks due to the reduction and oxidation of [Ru(SnPh$_3$)(CO)$_2$(iPr-DAB)]$_2$, respectively, were absent. These features allow one to conclude that the five-coordinate anion is directly formed *via* the two-electron reduction of parent Ru(Cl)(SnPh$_3$)(CO)$_2$(iPr-DAB), excluding the participation of the dimer [Ru(SnPh$_3$)(CO)$_2$(iPr-DAB)]$_2$ as a reducible intermediate.

Any ambiguity about the initial electron-transfer/chemical steps in the two-electron reduction path of [Ru(Cl)(SnPh$_3$)(CO)$_2$(iPr-DAB)] summarized in Scheme 1 (the ECEC route A and the ECE route B) can be eliminated considering the identical redox behavior of the related complexes Mn(Br)(CO)$_3$(iPr-DAB) and [Mn(CO)$_3$(iPr-DAB)]$^-$ discussed in the companion article.[5] The primary reduction step of Ru(Cl)(SnPh$_3$)(CO)$_2$(iPr-DAB), localized on the LUMO (lowest unoccupied molecular orbital) possessing a dominant $\pi^*_{(iPr-DAB)}$ character with minor contributions from $d_{yz(Ru)}$, $sp^3_{(SnPh_3)}$, and $p_{(Cl)}$ orbitals,[1a] yields the unstable radical anions [Ru(Cl)(SnPh$_3$)(CO)$_2$(iPr-DAB)]$^{\bullet-}$ which rapidly decompose to five-coordinate [Ru(SnPh$_3$)(CO)$_2$(iPr-DAB)]$^\bullet$. The $\delta(E_{p,c}) - \delta(\log(\nu))$ function in Figure 5, (Supporting

Table 2. ^{1}H, ^{13}C, and ^{119}Sn NMR Chemical Shifts (ppm) and Coupling Constants (in Parentheses (Hz)) of Ru(Cl)(SnPh$_3$)(CO)$_2$(iPr-DAB) and Its Reduction Products in THF-d_8 at Room Temperature

compound	imine H (s/d)[a]	SnC_6H_6 (m)[b]	SnC_6H_6 (m)[c]	$CH(CH_3)_2$ (sept)[d]	$CH(CH_3)_2$ (d)[d]	$CH(CH_3)_2$ (d)[d]	CO	*NC*[g]	Sn*C*	Sn*CCC*	Sn*CCCC*	*CH*(CH$_3$)$_2$	(*C*H$_3$)	^{119}Sn
Ru(Cl)(SnPh$_3$)(CO)$_2$(iPr-DAB)	8.22 (8.2)	7.4	7.3	4.25 (6.0)	1.43 (6.0)	1.01 (6.0)	203.1	161.9	145.1 (280)[h]	139.3 (35.5)[h]	130.2 (40.7)[h]	130.0(9.0)[h]	66.8	25.7/23.5	−50 (C_6D_6)
[Ru(Me)(CO)$_2$(iPr-DAB)]$_2$[e]	7.95			4.57 (6.6)	1.32 (6.7)	1.30 (6.5)									
[Ru(SnPh$_3$)(CO)$_2$(iPr-DAB)]$_2$	8.06 (17.4)	7.4	7.2	4.40 (6.5)	1.23 (6.5)	1.13 (6.5)	208.6	147.7	147.3	139.5	129.6	129.0	63.5	28.8/24.6	−53 (THF)
[Ru(SnPh$_3$)(CO)$_2$(iPr-DAB)]$^-$	6.91 (19.5)	7.3	7.0	4.49 (6.5)	1.24 (6.5)		217.8	125.8	151.4 (~250)[h]	137	126.4	126.1	61.5	~26	−4 (THF)
Ru(SnPh$_3$)$_2$(CO)$_2$(iPr-DAB)[f]	7.91 (26.1)	7.4	7.2	4.46 (6.5)	0.98 (6.5)		206.9 (55.8)[h]	151.8	145.6 (287)[h]	139.3 (36.2)[h]	129.7 (21.8)[h]	129.4	66.5	26.3	−53 (C_6D_6)

[a] Singlet (85%) and doublet (15%) due to the $^4J(^{117/119}Sn,H)$ coupling. [b] Ortho protons. [c] Meta/para protons. [d] Septet and doublet due to the $^3J(H,H)$ coupling. [e] C*H*$_3$ signal at 0.09 ppm; from ref 20. [f] From refs 7b and 8. [g] Imine carbon. [h] $J(^{117,119}Sn,^{13}C)$.

Table 3. Electrode Potentials of 2×10^{-3} M Ru(E)(E′)(CO)$_2$(iPr-DAB)[a]

complex	$E_{p,c}$[b] (V)[d]	$E_{1/2}$	$E_{p,a}$[c] (V)[d]
Ru(Cl)(PbPh$_3$)(CO)$_2$(iPr-DAB)	−1.60		0.80[e]
Ru(Cl)(SnPh$_3$)(CO)$_2$(iPr-DAB)	−1.48		
	−1.34[e]		0.80[e]
Ru(Cl)(Me)(CO)$_2$(iPr-DAB)[f]	−1.55		
Ru(PbPh$_3$)$_2$(CO)$_2$(iPr-DAB)	−1.74	−1.69	0.37
Ru(GePh$_3$)(SnPh$_3$)(CO)$_2$(iPr-DAB)	−1.78	−1.72	0.34
Ru(SnPh$_3$)$_2$(CO)$_2$(iPr-DAB)	−1.91	−1.86	0.34
Ru(Me)(SnPh$_3$)(CO)$_2$(iPr-DAB)	−1.98	−1.92	0.28
[Ru(PbPh$_3$)(CO)$_2$(iPr-DAB)]$_2$	−1.76		−0.10
[Ru(SnPh$_3$)(CO)$_2$(iPr-DAB)]$_2$	−1.68		−0.16
	−1.57[e]		−0.10[e]
[Ru(Me)(CO)$_2$(iPr-DAB)]$_2$[g]	−1.88		−0.37
[Ru(PbPh$_3$)$_2$(CO)$_2$(iPr-DAB)]$^{\bullet-}$	−2.31		
[Ru(SnPh$_3$)$_2$(CO)$_2$(iPr-DAB)]$^{\bullet-}$	<−2.8[h]		
[Ru(GePh$_3$)(SnPh$_3$)(CO)$_2$(iPr-DAB)]$^{\bullet-}$	−2.62		
[Ru(Me)(SnPh$_3$)(CO)$_2$(iPr-DAB)]$^{\bullet-}$	−2.71		
[Ru(PbPh$_3$)(CO)$_2$(iPr-DAB)]$^-$			−1.23
[Ru(SnPh$_3$)(CO)$_2$(iPr-DAB)]$^-$			−1.07
[Ru(Me)(CO)$_2$(iPr-DAB)]$^-$ [g]			−1.65

[a] In THF/0.3 M Bu_4NPF_6 at room temperature, unless stated otherwise; $v = 100$ mV/s, Pt disk electrode. [b] Reduction of the complex. [c] Oxidation of the complex. [d] V *vs* $E_{1/2}$ (Fc/Fc$^+$); $E_{1/2}$ (Fc/Fc$^+$) = +0.575 V (in THF) and +0.425 V (in MeCN) *vs* SCE. [e] Measured in MeCN. [f] Reduction potential indentical with that reported for Ru(I)(Me)(CO)$_2$(iPr-DAB).[9,10,20] [g] From ref 10. [h] Not observed within the potential window available in THF.

Information), linear for $v \leq 2$ V/s with the slope of 28 ± 1 mV decade^{-1}, documents[22] that the dissociation of Cl$^-$ as the first-order reaction must be the rate-determining step in the E_rC_iE sequence completed with the instantaneous one-electron reduction of [Ru(SnPh$_3$)(CO)$_2$(iPr-DAB)]$^\bullet$ to [Ru(SnPh$_3$)(CO)$_2$(iPr-DAB)]$^-$. As argued[5] for [Mn(CO)$_3$(iPr-DAB)]$^\bullet$, [Ru(SnPh$_3$)(CO)$_2$(iPr-DAB)]$^\bullet$ also reduces more positively than the parent [Ru(Cl(SnPh$_3$)-(CO)$_2$(iPR-DAB)] and the consecutive dimerization of [Ru(SnPh$_3$)(CO)$_2$(iPr-DAB)]$^\bullet$ cannot compete[23] with the latter electron transfer. At scan rates $v > 2$ V/s the rate-determining step is the irreversible electron transfer (E_i) to Ru(Cl)(SnPh$_3$)(CO)$_2$(iPr-DAB), resulting in $-(\delta(E_{p,c}/\delta\log(v) = 50$ mV decade^{-1} (theoretically $30/\alpha n$ mV,[22] where $n = 1$ in our case).

According to the cyclic voltammograms of [Ru(Cl)-(SnPh$_3$)(CO)$_2$(iPr-DAB)] recorded at 293 and 223 K, see above, the reverse oxidation of the five-coordinate anion [Ru(SnPh$_3$)(CO)$_2$(iPr-DAB)]$^-$ at room temperature results in the overall transfer of one electron, producing the dimer [Ru(SnPh$_3$)(CO)$_2$(iPr-DAB)]$_2$, as also observed in the course of the corresponding spectroelectrochemical experiments. At 223 K, however, it turns to a two-electron process which only recovers parent Ru(Cl)-(SnPh$_3$)(CO)$_2$(iPr-DAB). The primary electron-transfer step in the sequence obviously yields, independent of the temperature, the five-coordinate radicals [Ru(SnPh$_3$)-(CO)$_2$(iPr-DAB)]$^\bullet$. Following Scheme 1, the oxidation path of [Ru(SnPh$_3$)(CO)$_2$(iPr-DAB)]$^-$ may split at this point into two possible routes. The route C + E + E(F) is identical with that operating in the case of the related anion [Mn(CO)$_3$(iPr-DAB)]$^-$ in the presence of Br$^-$.[5] In the key step C, a fraction of [Ru(SnPh$_3$)(CO)$_2$(iPr-DAB)]$^\bullet$ takes up a solvent molecule (MeCN) and converts to the

(22) Bard, A. J.; Faulkner, L. R. *Electrochemical Methods, Fundamentals and Applications*; Wiley & Sons: New York, 1980; Chapter 11.

(23) Amatore, C.; Savéant, J. M. *J. Electroanal. Chem., Interfacial Electrochem.* **1981**, *125*, 1.

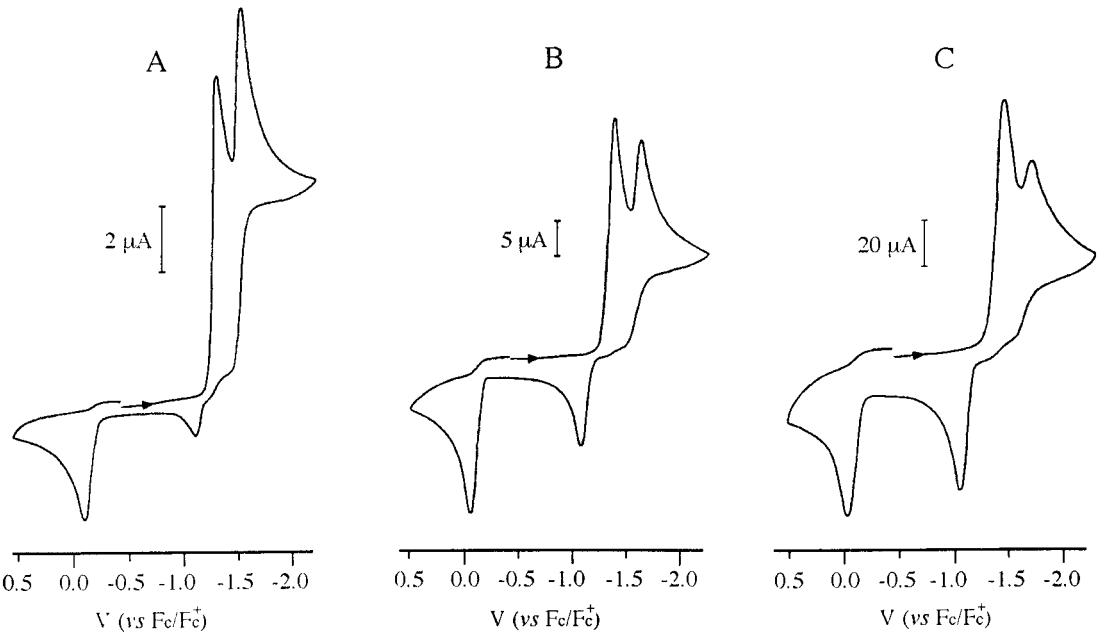

Figure 4. Cyclic voltammograms of Ru(Cl)(SnPh$_3$)(CO)$_2$(iPr-DAB) in MeCN at 293 K using a platinum disk microelectrode (d = 500 μm). Supporting electrolyte was 0.3 M Bu_4NPF_6. Scan rates (v): (A) 0.1V/s, (B) 1 V/s, (C) 10 V/s.

transient 18-electron radicals [Ru(MeCN)(SnPh$_3$)(CO)$_2$-(iPr-DAB)]$^\bullet$. In conformity with the arguments presented in the companion article,[5] in particular with the $\delta E_{p,c}$ *vs* log(v) and $\delta E_{p,a}$ *vs* log(v) trends for the reduction of Ru(Cl)(SnPh$_3$)(CO)$_2$(iPr-DAB) (see Figure 5) and the oxidation of [Ru(SnPh$_3$)(CO)$_2$(iPr-DAB)]$^-$, respectively, the latter solvento radicals instantaneously oxidize to the corresponding cations whose concomitant rapid reaction with the Cl$^-$ liberated during the reduction[24] recovers Ru(Cl)(SnPh$_3$)(CO)$_2$(iPr-DAB)]. Apparently, this route dominates at sufficiently *low temperatures*. At room temperature, Ru(Cl)(SnPh$_3$)(CO)$_2$(iPr-DAB) (and possibly also its precursor [Ru(MeCN)(SnPh$_3$)-(CO)$_2$(iPr-DAB)]$^+$) reacts with yet nonoxidized [Ru-(SnPh$_3$)(CO)$_2$(iPr-DAB)]$^-$, yielding ultimately the dimer [Ru(SnPh$_3$)(CO)$_2$(iPr-DAB)]$_2$, see routes E + F and E + G. Differently from [Mn(CO)$_3$(iPr-DAB)]$^-$, this ECEC sequence, however, *is not* the main oxidation route of [Ru(SnPh$_3$)(CO)$_2$(iPr-DAB)]$^-$ at *room temperature*, in agreement with the determined slope of the linear dependence of $\delta(E_{p,a})/\delta\log(v) = 23 \pm 2$ mV decade^{-1} (for v = 0.05−2 V/s). This value implies an overall $E_rC_i(E)$ sequence where the irreversible chemical step of [Ru-(SnPh$_3$)(CO)$_2$(iPr-DAB)]$^\bullet$ involves simultaneous pseudo-first-order (30 mV decade^{-1}) and second-order (20 mV decade^{-1})[22] reactions, corresponding, in Scheme 1, with routes C and D, respectively. The consecutive dimerization of [Ru(SnPh$_3$)(CO)$_2$(iPr-DAB)]$^\bullet$ (the dominant route D) becomes thermally quenched at 223 K, similar to the route E + F(G), see above. Identical reduction and reverse oxidation routes can be drawn for the corresponding complex Ru(Cl)(PbPh$_3$)(CO)$_2$(iPr-DAB).

UV−Vis and IR Spectroelectrochemistry of Ru(E)(E′)(CO)$_2$(iPr-DAB) (E = Me, SnPh$_3$, GePh$_3$, E′ = SnPh$_3$; E = E′ = PbPh$_3$). The near-UV−vis absorption maxima and IR ν(CO) wavenumbers of the title complexes Ru(E)(E′)(CO)$_2$(iPr-DAB) (E, E′ ≠ Cl) and their reduction products are collected in Table 1. The selected example of E = GePh$_3$, E′ = SnPh$_3$ is depicted in Figure 6 (Supporting Information).

The spectroelectrochemical experiments have confirmed that reduction of all of the non-halide title complexes produces the corresponding radical anions, in agreement with the conclusions of the previous study[8] of [Ru(SnPh$_3$)$_2$(CO)$_2$(iPr-DAB)]$^{\bullet-}$. The radical nature of [Ru(E)(E′)(CO)$_2$(iPr-DAB)]$^{\bullet-}$ was unequivocally confirmed by EPR spectroscopy, see Table 4. The representative EPR spectra of [Ru(GePh$_3$)(SnPh$_3$)(CO)$_2$(iPr-DAB)]$^{\bullet-}$ and [Ru(Me)(SnPh$_3$)(CO)$_2$(iPr-DAB)]$^{\bullet-}$ are depicted in Figures 7 and 8, respectively. All of the radical anions [Ru(E)(E′)(CO)$_2$(iPr-DAB)]$^{\bullet-}$ obtained on reducing the parent complexes with 1% Na(Hg) were sufficiently thermally stable with regard to the time needed to record a reasonably good EPR spectrum.

Subsequent electron transfer to [Ru(E)(E′)(CO)$_2$(iPr-DAB)]$^{\bullet-}$, E, E′ ≠ Cl, produced identical anionic species as those obtained during the two-electron cathodic step of Ru(Cl)(E′)(CO)(iPr-DAB) (E′ = SnPh$_3$, PbPh$_3$), *i.e.*, [Ru(E′)(CO)$_2$(iPr-DAB)]$^-$ (see Table 1). It is noteworthy that the reduction of [Ru(GePh$_3$)(SnPh$_3$)(CO)$_2$(iPr-DAB)]$^{\bullet-}$, see Figure 6, may afford both [Ru(SnPh$_3$)(CO)$_2$-(iPr-DAB)]$^-$ and [Ru(GePh$_3$)(CO)$_2$(iPr-DAB)]$^-$, as the Ru−SnPh$_3$ and Ru−GePh$_3$ bonds possess comparable strength. This property was confirmed on irradiation of Ru(GePh$_3$)(SnPh$_3$)(CO)$_2$(iPr-DAB) in CDCl$_3$, which led to a 40/60 mixture of Ru(Cl)(GePh$_3$)(CO)$_2$(iPr-DAB) and Ru(Cl)(SnPh$_3$)CO)$_2$(iPr-DAB).[21] In view of the almost identical ν(CO) wavenumbers and UV−vis spectra of [Ru(SnPh$_3$)$_2$(CO)$_2$(iPr-DAB)]$^{\bullet-}$ and [Ru(GePh$_3$)(SnPh$_3$)-(CO)$_2$(iPr-DAB)]$^{\bullet-}$, we may anticipate that [Ru(E′)(CO)$_2$-(iPr-DAB)]$^-$ (E′ = SnPh$_3$, GePh$_3$) also do not deviate substantially in their UV−vis and ν(CO) features and, therefore, cannot be distinguished in Figure 6.

For the complexes Ru(E)(E′)(CO)$_2$(iPr-DAB) (E = Me, E′ = SnPh$_3$; E = E′ = PbPh$_3$), the ultimate two-electron-reduction products [Ru(E′)(CO)$_2$(iPr-DAB)]$^-$ (E′ = Sn-Ph$_3$, PbPh$_3$) were already formed in a small amount along with a major amount of [Ru(E)(E′)(CO)$_2$(iPr-

(24) The Cl$^-$ anions may remain adsorbed at the surface of the Pt disk electrode, see for example: Osella, D.; Ravera, D.; Kukharenko, S. V.; Strelets, V. V.; Housecroft, C. E. *J. Organomet. Chem.* **1991**, *417*, 421.

Scheme 1

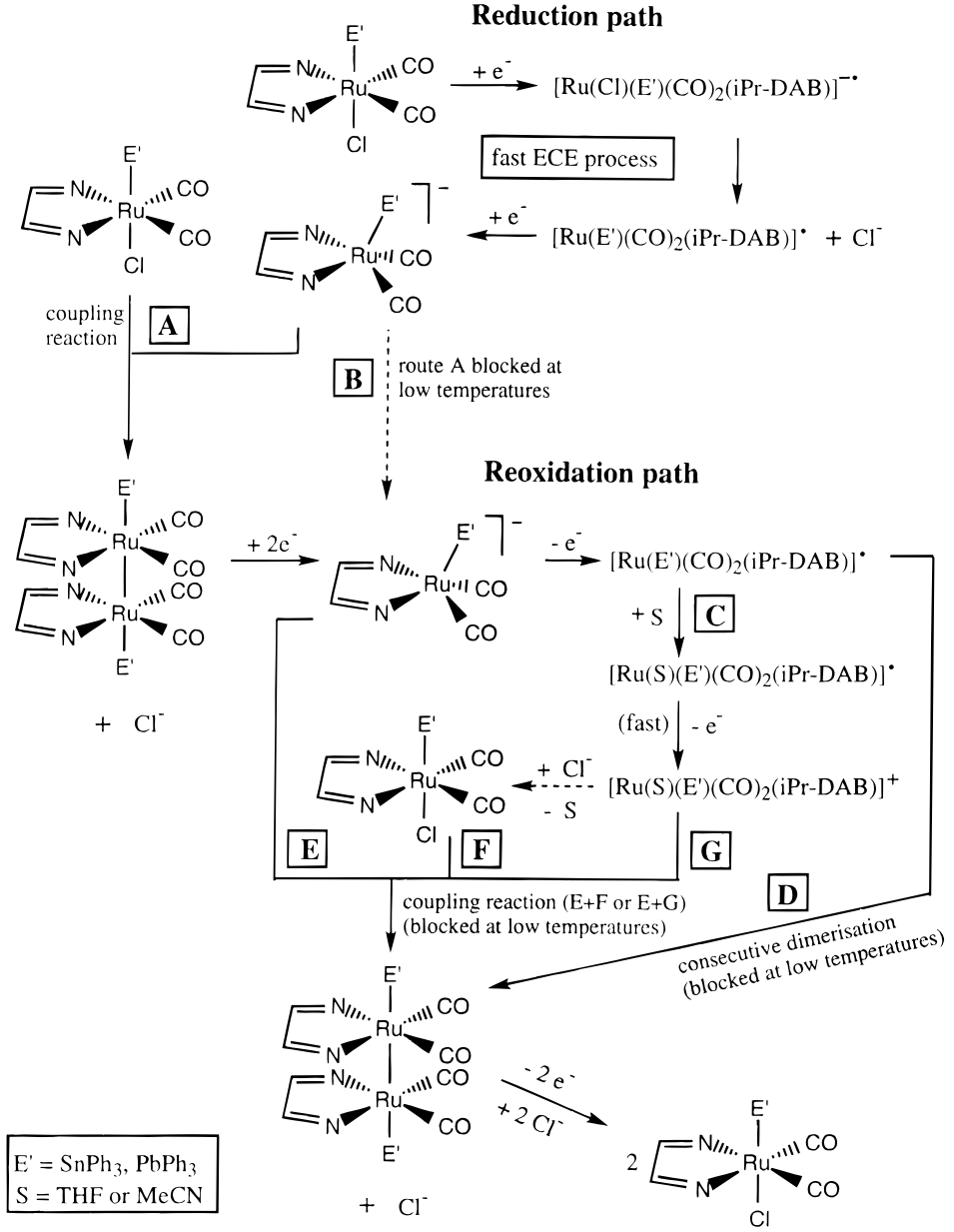

DAB)]•⁻ during the *first* cathodic step, probably due to slow cleavage of the Ru−E bond (see below). The apparent difference in the Ru−Sn and Ru−Me bond strength is also clearly illustrated by the complete absence of the alternative anionic product $[Ru(Me)(CO)_2(iPr\text{-}DAB)]^-$ (see Table 1).[9,10,20] We can conclude that the stability of the Ru−E bond in the one-electron- and two-electron-reduced species decreases in the order Ru−$SnPh_3$ ≈ Ru−$GePh_3$ > Ru−$PbPh_3$ > Ru−Me >> Ru−Cl.

Cyclic Voltammetry and Reduction Path of Ru(E)(E′)(CO)$_2$(iPr-DAB) (E = Me, $GePh_3$, $SnPh_3$, E′ = $SnPh_3$; E = E′ = $PbPh_3$). The cyclic voltammetric responses of the complexes Ru(E)(E′)(CO)$_2$(iPr-DAB) (E, E′ ≠ Cl), see Table 4, substantially deviate from those described above for the Cl derivatives. The representative cyclic voltammogram of $Ru(PbPh_3)_2(CO)_2(iPr\text{-}DAB)$ is depicted in Figure 9. The non-halide complexes are reduced in a chemically reversible one-electron step to the corresponding radical anions, in conformity with the EPR spectra of the latter species recorded on a longer time scale of minutes, see above. The electrochemical reversibility of this cathodic step has been documented by the identical ΔE_p values of both $[Ru(E)(E')(CO)_2(iPr\text{-}DAB)]^{0/\bullet-}$ and Fc/Fc^+ redox couples at comparable concentrations and by $\delta E_{p,c}/\delta\log(\nu) = 0$ for $\nu = 0.05-1$ V/s. The rather negative second cathodic peak in the cyclic voltammograms (see Figure 9) belongs to the irreversible reduction of $[Ru(E)(E')(CO)_2(iPr\text{-}DAB)]^{\bullet-}$ which produces, as revealed by the IR and UV−vis OTTLE experiments, the five-coordinate anions $[Ru(E')(CO)_2(iPr\text{-}DAB)]^-$ (E′ = $SnPh_3$, $PbPh_3$).

The events along the reduction path of Ru(E)(E′)(CO)$_2$(iPr-DAB) (E, E′ ≠ Cl) are summarized in Scheme 2. During the OTTLE electrolysis, the radical anions $[Ru(PbPh_3)_2(CO)_2(iPr\text{-}DAB)]^{\bullet-}$ and $[Ru(Me)(SnPh_3)(CO)_2(iPr\text{-}DAB)]^{\bullet-}$ probably undergo slow dissociation of the $PbPh_3^\bullet$ and Me• ligands, yielding the five-coordinate anions $[Ru(PbPh_3)(CO)_2(iPr\text{-}DAB)]^-$ and $[Ru(SnPh_3)(CO)_2(iPr\text{-}DAB)]^-$ directly, respectively. This secondary chemical reaction has also been reported for the related radical anion $[Mn(Me)(CO)_3(iPr\text{-}DAB)]^{\bullet-}$.[5] The radical anions $[Ru(PbPh_3)_2(CO)_2(iPr\text{-}DAB)]^{\bullet-}$ and $[Ru(Me)(SnPh_3)(CO)_2(iPr\text{-}DAB)]^{\bullet-}$ were, however, found to de-

Table 4. EPR Parameters of [Ru(E)(E′)(CO)$_2$(iPr-DAB)]$^{\bullet-}$ Obtained *via* Reduction of the Parent Complexes with 1% Na(Hg) in THF at 293 K

nuclei	no.	natural abundance (%)	spin	A_{iso} (G)[g]	E = GePh$_3$, E' = SnPh$_3$ (G)[a,b]	E = GePh$_3$, E' = SnPh$_3$ (G)[a]	E = Me, E' = SnPh$_3$ (G)[a]	E = PbPh$_3$, E' = PbPh$_3$ (G)[a]
^{99}Ru	1	12.7	$^5/_2$		5.7 (4.1)	5.34	(3.9) *f*	*f*
^{101}Ru	1	17.1	$^5/_2$		6.4 (4.6)	6.00	(4.3) *f*	*f*
^{117}Sn	1 or 2	7.6	$^1/_2$	−6669	317 (344)	350	∼3700 (401)	
$^{117}Sn/A_{iso}$					*0.047*	*0.052*	*∼0.055*	
^{119}Sn	1 or 2	8.6	$^1/_2$	−7268	332 (360)	366	∼370 (419)	
$^{117}Sn/A_{iso}$					*0.047*	*0.050*	*∼0.055*	
^{207}Pb	1 or 2	22.6	$^1/_2$	+6868				∼570
$^{207}Pb/A_{iso}$								*0.083*
^{73}Ge	1	7.6	$^9/_2$	−535		14.6		
$^{73}Ge/A_{iso}$						*0.027*		
^{14}N	2	99.6	1		8.20 (11.6)	8.00	7.95 (11.0)	∼7.5[f]
^{1}H[c]	2	99.9	$^1/_2$		3.55 (4.3)	4.29	3.62 (4.4)	∼4.0[f]
^{1}H[d]	2	99.9	$^1/_2$		3.25	3.71	2.69	∼3.3[f]
^{1}H[e]	3	99.9	$^1/_2$				0.68 (1.5)	
g-factor					1.9960	1.9968	1.9986	1.9919

[a] Hyperfine coupling constants based on the simulated values,[11] except for the $^{117/119}$Sn and ^{207}Pb hyperfine coupling constants which were derived from the experimental spectra using the correction factors taken from ref 33. The values in parentheses are the hyperfine coupling constants calculated[19] from the theoretical spin-density distribution obtained from the DFT-MO calculations.[1a,8] [b] From ref 8. [c] Imine protons. (We assume that also in this case a_H(CH=N(iPr)) > a_H(C*H*(CH$_3$)$_2$), in accordance with the data presented in ref 8). [d] (C*H*(CH$_3$)$_2$). [e] Ru−C*H*$_3$. [f] These values could not be (accurately) determined due to a large natural line width for [Ru(PbPh$_3$)$_2$(CO)$_2$(iPr-DAB)]$^{\bullet-}$ or poor signal-to-noise ratio for [Ru(Me)(SnPh$_3$)(CO)$_2$(iPr-DAB)]$^{\bullet-}$. [g] A_{iso} = theoretical isotropic coupling constants for free ions; according to ref 33.

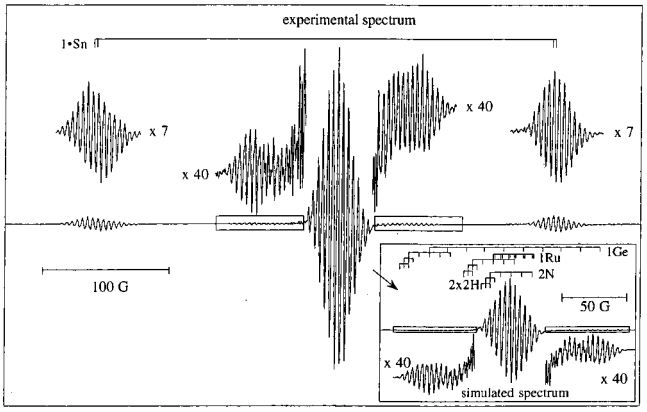

Figure 7. EPR spectrum of [Ru(GePh$_3$)(SnPh$_3$)(CO)$_2$(iPr-DAB)]$^{\bullet-}$ in THF at room temperature, generated by in-situ reduction of the corresponding parent complex with 1% Na-(Hg) (modulation amplitude 0.5 G; attenuation 10 dB.)

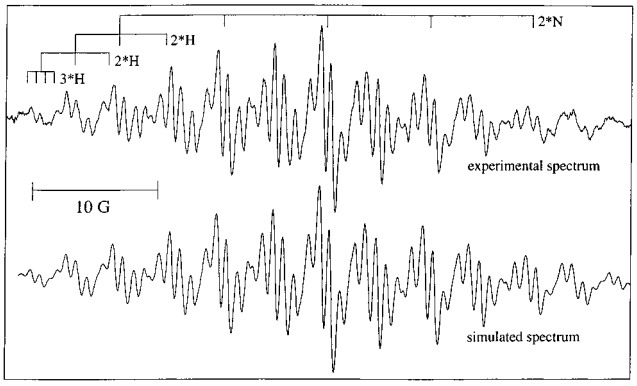

Figure 8. EPR spectrum of [Ru(Me)(SnPh$_3$)(CO)$_2$(iPr-DAB)]$^{\bullet-}$ generated in THF at room temperature by in-situ reduction of the corresponding parent complex with 1% Na-(Hg) (modulation amplitude 0.5 G; attenuation 10 dB; doublet side lines due to the $^{117/119}$Sn coupling not shown).

compose more slowly when generated by reduction of the parent complexes with sodium amalgam. This difference might be ascribed to a stabilizing ion-pairing effect of the Na$^+$ countercation. The fate of the free Me$^\bullet$ and PbPh$_3^\bullet$ radicals remained unclear, as they could not

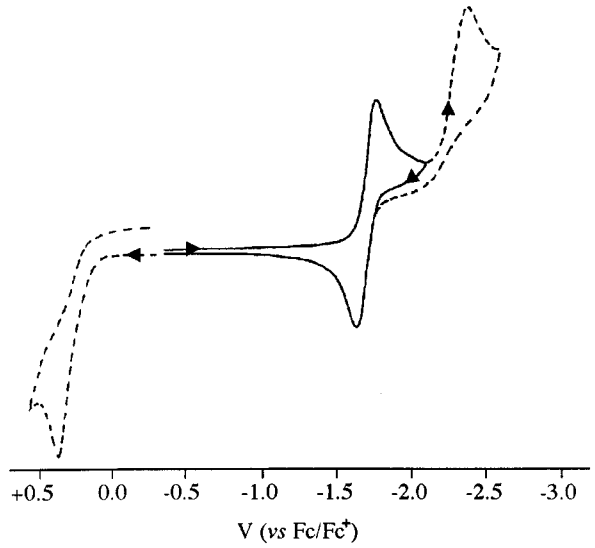

Figure 9. Cyclic voltammogram of Ru(PbPh$_3$)$_2$(CO)$_2$(iPr-DAB) in THF at 293 K using a platinum disk microelectrode (d = 500 μm). The supporting electrolyte was 0.3 M Bu$_4$NPF$_6$.

Scheme 2

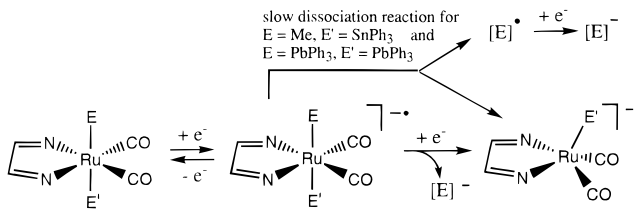

be detected by conventional EPR spectroscopy. The pronounced tendency of the Me and PbPh$_3$ ligands to dissociate was also observed on irradiation of these Ru-(E)(E′)(CO)$_2$(iPr-DAB) complexes.[21]

The chemically irreversible oxidation of Ru(E)(E′)-(CO)$_2$(iPr-DAB) (E, E′ ≠ Cl), localized on the $\sigma_{(E-Ru-E')}$ orbital,[1a,8] is shifted considerably more negatively relative to the oxidation of Ru(Cl)(E′)(CO)$_2$(iPr-DAB), see Figure 9 and Table 3. This process was not studied in detail.

Discussion

In this article we demonstrate that, similarly to the photochemical[21] and photophysical[1a] properties, the redox behavior of the title Ru(E)(E′)(CO)$_2$(iPr-DAB) complexes is also strongly influenced by the strength of the axial covalent E−Ru−E′ bonds and by the variable extent of mixing between the $\sigma_{(E-Ru-E')}$ and $\pi^*_{(iPr-DAB)}$ orbitals.

Differences in Reduction Paths of Ru(Cl)(E′)(CO)$_2$(iPr-DAB) (E′ = SnPh$_3$, PbPh$_3$) and Ru(Cl)(Me)(CO)$_2$(iPr-DAB). The spectroelectrochemical results obtained for Ru(Cl)(SnPh$_3$)(CO)$_2$(iPr-DAB) show that its reduction path in Scheme 1 is not valid for the derivative Ru(Cl)(Me)(CO)$_2$(iPr-DAB).[9,10,20] The only common point is the first electron-transfer/Cl$^-$-loss step which produces the unstable radicals [Ru(Cl)(E′)(CO)$_2$(iPr-DAB)]$^{\bullet-}$ and [Ru(E′)(CO)$_2$(iPr-DAB)]$^\bullet$ (E′ = Me, SnPh$_3$). The driving force of this secondary chemical reaction has its origin in the partial delocalization of the electron density from the largely π^*(iPr-DAB) SOMO to the σ^*(Ru−Cl) orbital.[1a,f] In butyronitrile (nPrCN) at low temperatures, the 18-electron radicals [Ru(nPrCN)(Me)(CO)$_2$(iPr-DAB)]$^\bullet$ could be stabilized. At ambient temperature, the radicals [Ru(Me)(CO)$_2$(iPr-DAB)]$^\bullet$ directly dimerize. Both [Ru(Me)(CO)$_2$(iPr-DAB)]$_2$ and [Ru(nPrCN)(Me)(CO)$_2$(iPr-DAB)]$^\bullet$ are ultimately reduced to [Ru(Me)(CO)$_2$(iPr-DAB)]$^-$.

Importantly, the $\delta E_p/\delta\log(\nu)$ trends in cyclic voltammetry predict that the $E_{1/2}$ potential of the [Ru(SnPh$_3$)(CO)$_2$(iPr-DAB)]$^{-/\bullet}$ redox couple lies *more positively* than that of the [Ru(Cl)(SnPh$_3$)(CO)$_2$(iPr-DAB)]$^{0/\bullet-}$ redox couple. As a consequence, [Ru(SnPh$_3$)(CO)$_2$(iPr-DAB)]$^\bullet$ is directly reduced to [Ru(SnPh$_3$)(CO)$_2$(iPr-DAB)]$^-$ at the applied reduction potential of Ru(Cl)(SnPh$_3$)(CO)$_2$(iPr-DAB). The consecutive dimerization of the [Ru(SnPh$_3$)(CO)$_2$(iPr-DAB)]$^\bullet$ radicals, thus, cannot compete with the electron-transfer step,[23] and the dimer [Ru(SnPh$_3$)(CO)$_2$(iPr-DAB)]$_2$ is only produced by the temperature-controlled nucleophilic attack of [Ru(SnPh$_3$)(CO)$_2$(iPr-DAB)]$^-$ at the parent complex Ru(Cl)(SnPh$_3$)(CO)$_2$(iPr-DAB).

In contrast, the one-electron reduction path of Ru(Cl)(Me)(CO)$_2$(iPr-DAB) implies that the transient five-coordinate radicals [Ru(Me)(CO)$_2$(iPr-DAB)]$^\bullet$ are reduced *more negatively* than the parent Cl complex. In view of the rather similar reduction potentials of Ru(Cl)(E′)(CO)$_2$(iPr-DAB) (E′ = Me, SnPh$_3$), see Table 4, the key factor must be a profound difference between the $E_{1/2}$ potentials of the five-coordinate redox couples [Ru(E′)(CO)$_2$(iPr-DAB)]$^{\bullet/-}$ (E′ = Me, SnPh$_3$). The anion [Ru(Me)(CO)$_2$(iPr-DAB)]$^-$ is indeed oxidized significantly more negatively than the SnPh$_3$ derivative, see Table 3. For this reason the oxidation of [Ru(Me)(CO)$_2$(iPr-DAB)]$^-$ in RCN (R = Me, nPr) at low temperatures yields the radicals [Ru(RCN)(Me)(CO)$_2$(iPr-DAB)]$^\bullet$ mainly while [Ru(SnPh$_3$)(CO)$_2$(iPr-DAB)]$^-$ undergoes a two-electron oxidation producing the cations [Ru(RCN)(SnPh$_3$)(CO)$_2$(iPr-DAB)]$^+$. The higher energy of the HOMO of [Ru(Me)(CO)$_2$(iPr-DAB)]$^-$ relative to that of [Ru(SnPh$_3$)(CO)$_2$(iPr-DAB)]$^-$ may indicate a lower stability of the former, less π-delocalized[5,25] anion. Indeed, [Ru(SnPh$_3$)(CO)$_2$(iPr-DAB)]$^-$ remains fairly stable in the presence of a large excess of PPh$_3$, while [Ru(Me)(CO)$_2$(iPr-DAB)]$^-$ decomposes[10] at room temperature to Ru^0(PPh$_3$)$_2$(CO)$_3$ and Ru^0(PPh$_3$)(CO)$_2$(iPr-DAB).

Electronic Structure of [Ru(E)(E′)(CO)$_2$(iPr-DAB)]O$^{\bullet-}$ (E = Me, GePh$_3$, SnPh$_3$, E′ = SnPh$_3$; E = E′ = PbPh$_3$). The electronic structure of the inherently stable radical anion [Ru(SnPh$_3$)$_2$(CO)$_2$(iPr-DAB)]$^{\bullet-}$ has been discussed in detail elsewhere.[8] The $\sigma_{(Sn-Ru-Sn)}$-$\pi^*_{(DAB)}$ electron delocalization responsible for the stability and very close bonding properties of the couple [Ru(SnPh$_3$)$_2$(CO)$_2$(iPr-DAB)]$^{0/\bullet-}$ also applies, on the basis of the UV−vis, IR, and EPR data, for the other complexes [Ru(E)(E′)(CO)$_2$(iPr-DAB)]$^{0/\bullet-}$ (E, E′ ≠ Cl) under study.

Notably, the EPR *g*-factors of the title radical anions [Ru(E)(E′)(CO)$_2$(iPr-DAB)]$^{\bullet-}$ are considerably smaller than the free-electron value $g_e = 2.0023$ due to a spin−orbit interaction given by the presence of the heavy Ru and group 14 metal (M(14)) atoms and due to an admixture of the higher unoccupied orbitals $\sigma^*_{(E-Ru-E')}$ into the π^* SOMO possessing significant contributions from the Ru and M(14) orbitals.[8] These arguments correspond with the smaller *g*-factors (i) on coordination of axial ligands containing heavier metals (Ge < Sn < Pb) and (ii) on decreasing the energetic separation between the π^* and σ^* frontier orbitals reflected in a lower-energy shift of the π^* SOMO → $\sigma^*_{(E-Ru-E')}$ absorption band[8] in the UV−vis spectra of [Ru(E)(E′)(CO)$_2$(iPr-DAB)]$^{\bullet-}$, *viz.* [Ru(PbPh$_3$)$_2$(CO)$_2$(iPr-DAB)]$^{\bullet-}$: g = 1.9919, λ_{max} = 812 nm; [Ru(SnPh$_3$)$_2$(CO)$_2$(iPr-DAB)]$^{\bullet-}$: g = 1.9960, λ_{max} = 652 nm; [Ru(SnPh$_3$)(GePh$_3$)(CO)$_2$(iPr-DAB)]$^{\bullet-}$: g = 1.9968, λ_{max} = 641 nm; [Ru(SnPh$_3$)(Me)(CO)$_2$(iPr-DAB)]$^{\bullet-}$: g = 1.9986, λ_{max} = 428 nm.

The $^{117/119}$Sn hyperfine splitting constant (a_{Sn}) is smaller for [Ru(SnPh$_3$)$_2$(CO)$_2$(iPr-DAB)]$^{\bullet-}$ than for [Ru(E)(SnPh$_3$)(CO)$_2$(iPr-DAB)]$^{\bullet-}$ with more polarized E−Ru−Sn bonds (E = Me, GePh$_3$). This also applies for the theoretical a_{Sn} constants (Table 3), derived from the DFT-MO calculations on [Ru(SnH$_3$)$_2$(CO)$_2$(H-DAB)]$^{\bullet-}$ [8] and [Ru(Me)(SnH$_3$)(CO)$_2$(H-DAB)]$^{\bullet-}$ (see Supporting Information). Indeed, these calculations predicted that the contribution of the single SnH$_3$ ligand to the SOMO of [Ru(Me)(SnH$_3$)(CO)$_2$(H-DAB)]$^{\bullet-}$ is larger than that of the methyl group and also than each of the SnH$_3$ ligands to the SOMO of [Ru(SnH$_3$)$_2$(CO)$_2$(H-DAB)]$^{\bullet-}$.

In order to relate the hyperfine splitting constants of the ^{73}Ge, ^{117,119}Sn, and ^{207}Pb nuclei (a_M), the experimental a_M values have been divided by the theoretical isotropic hyperfine splitting constants of the free ions. The larger values of a_M/A_{iso} reflect higher relative spin densities on the M(14) nuclei in the order Ge(0.027) < Sn(*ca.* 0.050) < Pb(0.083). This trend agrees with the increasing contributions expected from the more diffuse orbitals of the heavier M(14) elements to the SOMO of the radical anions.

Electronic and Geometric Structure of [Ru(SnPh$_3$)(CO)$_2$(iPr-DAB)]$^-$. Valuable information about the bonding properties of the closed-shell anion [Ru(SnPh$_3$)(CO)$_2$(iPr-DAB)]$^-$ can be derived from the NMR spectral data in Table 2. The effect of the two added electrons is best illustrated (i) in the ^{1}H NMR spectra by the upfield chemical shift of the signal due to the iPr-DAB imine protons from 7.9−8.3 ppm for the neutral SnPh$_3$ complexes, to 6.9 ppm for [Ru(SnPh$_3$)(CO)$_2$(iPr-DAB)]$^-$, and (ii) in the ^{13}C NMR spectra by the large upfield chemical shift of the N*C* signal from 150−160 ppm to 125.8 ppm in the same sequence. These upfield shifts are induced by increased electron

density in the lowest π^* orbital of the iPr-DAB ligand. The ^{1}H and ^{13}C NMR signals of the phenyl groups also shift slightly upfield, indicating partial localization of the negative charge on the phenyl rings of $SnPh_3$ as well, see Table 2 and Figure 3.

Due to the hindered rotation of the iPr-groups of iPr-DAB along the N−CH(CH$_3$)$_2$ bond, the ^{1}H NMR spectrum of the asymmetric complex Ru(Cl)($SnPh_3$)(CO)$_2$-(iPr-DAB) in Figure 3A exhibits two doublet signals of the methyl protons. For Ru($SnPh_3$)$_2$(CO)$_2$(iPr-DAB) with identical axial ligands, obviously only one doublet is observed, see Figure 3B. The methyl groups of iPr-DAB pointing toward the $SnPh_3$ ligand are directed toward the deshielding cone of the phenyl groups, and their signals are, therefore, considerably shifted to smaller values. Importantly, the ^{1}H NMR spectrum of the low-symmetry anion [Ru($SnPh_3$)(CO)$_2$(iPr-DAB)]$^-$ also shows only one CH(C*H*$_3$)$_2$ doublet at an averaged value of the two doublet signals of Ru(Cl)($SnPh_3$)(CO)$_2$-(iPr-DAB), see Figure 3C. From these data we conclude that the Ru($SnPh_3$)(CO)$_2$ unit freely rotates relative to the iPr-DAB ligand. Due to this fluxional process on the NMR time scale at room temperature, the four methyl groups become magnetically equivalent, resulting in only one CH(C*H*$_3$) doublet with a slightly increased natural line width. No attempts were made to determine the rotation barrier with the aid of low-temperature NMR spectroscopy. Due to the five-coordinate geometry of the anion, the $SnPh_3$ ligand is bent away from the iPr-DAB ligand. The methyl groups are, therefore, placed further away from the deshielding cones of the phenyl groups, resulting in a downfield shift of the methyl signals relative to those of Ru($SnPh_3$)$_2$-(CO)$_2$(iPr-DAB), see Table 2 and Figure 3.

The chemical shift of the ^{119}Sn nucleus in the neutral complexes Ru(E)($SnPh_3$)(CO)$_2$(iPr-DAB) (E = Cl, $SnPh_3$, (carbonyl)metal fragment) is typically *ca.* −50 ppm.[7] In contrast, $\delta = -4$ ppm is observed for [Ru($SnPh_3$)(CO)$_2$-(iPr-DAB)]$^-$ regardless of the increased negative charge. It is difficult to provide a straightforward explanation for this downfield shift owing to the unknown effects of the shielding and deshielding cones of the Ru(DAB) and phenyl rings on the position of the ^{119}Sn resonance signal.

Clear evidence for *delocalized* π-bonding in [Ru-($SnPh_3$)(CO)$_2$(iPr-DAB)]$^-$ has been gathered from its resonance Raman spectrum. On excitation into the lowest electronic transition at 503 nm, the main resonance Raman effect is observed the for bending modes of the Ru(DAB) metallacycle in the 800−950 cm^{-1} region,[1a,25,26] see Table 1. These Raman modes are not enhanced significantly on excitation into electronic transitions between strongly Ru/E′- and iPr-DAB-*localized* orbitals.[1a,2c] Their occurence therefore reveals delocalized bonding within the metal-DAB metallacycle.[1a,2c,25−30] At the same time, the resonance effect is rather weak due to a small overall excited-state distortion, distributed over many normal coordinates. These results thus clearly show that the resonant lowest-energy ($\pi_{HOMO} \rightarrow \pi^*_{LUMO}$)[1f,25] electronic transition of [Ru($SnPh_3$)(CO)$_2$(iPr-DAB)]$^-$ can be considered as having a strongly mixed d$\pi_{(Ru)}$ + $\pi^*_{(DAB)} \rightarrow \pi^*_{(DAB)}$ − d$\pi_{(Ru)}$ character. The extensive mixing between the frontier orbitals of the Ru($SnPh_3$)(CO)$_2$ fragment and the iPr-DAB ligand in the anion is also accompanied by a strong σ-donation from the reduced iPr-DAB ligand to the Ru($SnPh_3$) unit, contributing to the relatively large coupling constant $^4J(^{117/119}Sn,H_{imine}) = 19.5$ Hz determined from the ^{1}H NMR spectrum of [Ru($SnPh_3$)-(CO)$_2$(iPr-DAB)]$^-$, see Table 2.

The redox series Ru($SnPh_3$)$_2$(CO)$_2$(iPr-DAB)/[Ru-($SnPh_3$)$_2$(CO)$_2$(iPr-DAB)]$^{\bullet-}$/[Ru($SnPh_3$)(CO)$_2$(iPr-DAB)]$^-$, thus, consists of complexes with a strongly delocalized electronic structure. The six-coordinate complexes are characterized by a delocalization of the σ-electron density along the 3-center, 4-electron $\sigma_{(Sn-Ru-Sn)}$ bond and further on the iPr-DAB ligand *via* an extensive mixing of the Ru(5p$_z$) + 2Sn(sp^3) + DAB(π^*) characters.[8] In contrast, the bonding properties of [Ru($SnPh_3$)(CO)$_2$-(iPr-DAB)]$^-$ are markedly determined by the strong σ,π-donor capacity of the reduced iPr-DAB ligand typically exerted in a five-coordinate complex.[5,25,31] A similar conclusion can be drawn for the other non-halide [Ru-(E)(E′)(CO)$_2$(iPr-DAB)]$^{0/\bullet-}$ and [Ru(E)(CO)$_2$(iPr-DAB)]$^-$ complexes.

Acknowledgment. The Dutch group gratefully appreciates financial support from the Netherlands Foundation for Chemical Research (SON) and the Netherlands Organization for Pure Research (NWO). The French group acknowledges partial support from CNRS, Ecole Normale Supérieure, and the French Ministry of Research.

Supporting Information Available: A table of DFT-calculated characters and energies of the relevant MOs of [Ru-(Me)(SnH_3)(CO)$_2$(H-DAB)]$^{\bullet-}$ and Figures 3, 5, and 6 showing the NMR spectra of Ru(E)($SnPh_3$)(CO)$_2$(iPr-DAB) (E = Cl, $SnPh_3$) and [Ru($SnPh_3$)(CO)$_2$(iPr-DAB)]$^-$, $E_{p,c}$ *vs* log(v) and $I_p v^{-1/2}$ *vs* log(v) functions of Ru(Cl)($SnPh_3$)(CO)$_2$(iPr-DAB), and IR and UV−vis spectra recorded during the reduction of Ru-($GePh_3$)($SnPh_3$)(CO)$_2$(iPr-DAB), respectively (4 pages). Ordering information is given on any current masthead page.

OM9702800

(25) Hartl, F.; Baerends, E. J.; Rossenaar, B. D.; Stufkens, D. J.; Wilms, M. P. Manuscript in preparation.
(26) Kokkes, M. W.; Stufkens, D. J.; Oskam, A. *J. Chem. Soc., Dalton Trans.* **1983**, *439*, 861.
(27) Aarnts, M. P.; Wilms, M. P.; Stufkens, D. J.; Baerends, E. J.; Vlček, A., Jr. *Organometallics* **1997**, *16*, 2055.
(28) Kokkes, M. W.; Snoeck, T. L.; Stufkens, D. J.; Oskam, A.; Christophersen, M.; Stam, C. H. *J. Mol. Struct.* **1985**, *131*, 11.
(29) Rossenaar, B. D.; Kleverlaan, C. J.; van de Ven, M. C. E.; Stufkens, D. J.; Oskam, A.; Goubitz, K.; Fraanje, J. *J. Organomet. Chem.* **1995**, *493*, 153.
(30) Kaesz, H. D.; Bau, R.; Hendrickson, D.; Smith, J. M. *J. Am. Chem. Soc.* **1967**, *89*, 2844.
(31) (a) Hartl, F.; Vlček, A., Jr.; deLearie, L. A.; Pierpont, C. G. *Inorg. Chem.* **1990**, *29*, 1073. (b) Hartl, F.; Stufkens, D. J.; Vlček, A.,Jr. *Inorg. Chem.* **1992**, *31*, 1687. (c) Hartl, F. *Inorg. Chim. Acta*, in press.
(32) Cotton, F. A.; Kraihanzel, C. S. *J. Am. Chem. Soc.* **1962**, *84*, 4432.
(33) Goodman, B. A.; Raynor, J. B. *Adv. Inorg. Chem. Radiochem.* **1970**, *13*, 135.